

# Neural-network quantum state study of the long-range antiferromagnetic Ising chain

Jicheol Kim,<sup>1</sup> Dongkyu Kim,<sup>1,2</sup> and Dong-Hee Kim<sup>1,\*</sup>

<sup>1</sup>*Department of Physics and Photon Science, Gwangju Institute of Science and Technology, Gwangju 61005, Korea*

<sup>2</sup>*Kakao Corporation, Pango, Gyeonggi 13529, Korea*

We investigate quantum phase transitions in the transverse field Ising chain with algebraically decaying long-range antiferromagnetic interactions by using the variational Monte Carlo method with the restricted Boltzmann machine being employed as a trial wave function ansatz. In the finite-size scaling analysis with the order parameter and the second Rényi entropy, we find that the central charge deviates from  $1/2$  at a small decay exponent  $\alpha_{\text{LR}}$  in contrast to the critical exponents staying very close to the short-range (SR) Ising values regardless of  $\alpha_{\text{LR}}$  examined, supporting the previously proposed scenario of conformal invariance breakdown. To identify the threshold of the Ising universality and the conformal symmetry, we perform two additional tests for the universal Binder ratio and the conformal field theory (CFT) description of the correlation function. It turns out that both indicate a noticeable deviation from the SR Ising class at  $\alpha_{\text{LR}} < 2$ . However, a closer look at the scaled correlation function for  $\alpha_{\text{LR}} \geq 2$  shows a gradual change from the asymptotic line of the CFT verified at  $\alpha_{\text{LR}} = 3$ , providing a rough estimate of the threshold being in the range of  $2 \lesssim \alpha_{\text{LR}} < 3$ .

## I. INTRODUCTION

Artificial neural networks and machine learning have been influencing the paradigm of physics research with a growing number of applications on various subjects, including phase transitions and critical phenomena in classical and quantum many-body systems [1–4]. In particular, the representation of a quantum wave function by a neural network [5] provides an alternative numerical platform combined with the variational Monte Carlo (VMC) method to find the ground state of a many-body Hamiltonian. The neural-network quantum state (NQS) has extended its area of applications to the Fermi and Bose Hubbard models [6, 7], real-time dynamics [5, 8], open quantum systems [9–12], quantum state tomography [13, 14], frustrated systems [15–21], and *ab initio* simulations of molecules [22–24]. The NQS ansatz offers the high expressive capacity often measured in terms of entanglement scaling [25–29], proposing a complementary tool to conventional numerical methods for studying quantum criticality.

In this paper, we investigate quantum phase transitions in the transverse field Ising chain (TFIC) with algebraically decaying long-range (LR) antiferromagnetic (AF) interactions by employing the NQS ansatz for the VMC calculations. LR-interacting quantum systems have attracted growing attention, both theoretical and experimental [30]. The trapped-ion quantum simulation [31] realized the TFIC Hamiltonian with an LR interaction that maps to the form of  $1/r^{\alpha_{\text{LR}}}$  with a tunable exponent  $\alpha_{\text{LR}}$ , providing a controllable experimental platform to study quantum phase transitions at and out of equilibrium [32–34]. The nearest-neighbor-interacting short-range (SR) TFIC is a textbook example of quantum critical behavior in one dimension (1D) that belongs to the universality class of the classical two-dimensional (2D) Ising model [35]. However, such quantum-classical correspondence to the universality of critical phenomena becomes nontrivial in presence of LR interactions. A central question of how criticality depends on  $\alpha_{\text{LR}}$  is still an active subject of various numerical and analytical

studies [30, 36–62].

We revisit this question in the AF side of the LR interactions for TFIC where the breakdown of the Ising class in the critical ground state seems to be very different from what is established in the ferromagnetic (FM) counterpart [47–52, 56–58]. Because an exact solution is not available, constructing the picture of how its criticality deviates from the Ising class as  $\alpha_{\text{LR}}$  decreases relies primarily on the collection of numerical observations. Despite various numerical studies characterizing the quantum phase transition in AF-LR-TFIC at equilibrium [53–57, 59] and out of equilibrium [56, 60], the picture remains incomplete in some parts, which requires more numerical evidence for clarification. Using the restricted Boltzmann machine (RBM) for the NQS ansatz [5], we consider the moments of staggered magnetization including the order parameter and the Binder ratio, the two-point correlation function, and the entanglement entropy to examine the present picture and find clearer signatures of the breakdown of the SR Ising class and the conformal invariance along the critical line.

We begin with brief reviews of previous results on the characterization of the criticality. The first study of AF-LR-TFIC [53] using the time-dependent variational principle (TDVP) found a phase transition for all  $\alpha_{\text{LR}} > 0$ , where it turned out that the critical exponent of the correlation function decreases from the SR Ising value for  $\alpha_{\text{LR}} \lesssim 2$ . A significant increase in the central charge from the Ising value  $1/2$  was observed at  $\alpha_{\text{LR}} \lesssim 1$  in the TDVP [53] and density matrix renormalization group (DMRG) [54] calculations, based on which the breakdown of conformal invariance was proposed [54]. While here we focus on the critical ground state, a violation of the area law for the entanglement entropy was observed in the offcritical area [53, 54, 59], and it was shown that the area law of the noncritical ground state holds for  $\alpha_{\text{LR}} > 2$  [63].

On the other hand, contrasting evidence was found in the other DMRG calculations [55, 56], where the estimates of the critical exponents  $\nu \simeq 1$  and  $\beta \simeq 1/8$  and the dynamic exponent  $z \simeq 1$  were in agreement with the SR Ising values for all examined  $\alpha_{\text{LR}}$  between 0.4 and 3. Although, these DMRG estimates of the critical exponents have not been fully verified in different approaches. Linked cluster expansion calculations [57] reported  $z\nu = 1.7(5)$  for  $\alpha_{\text{LR}} = 2$  while

\* dongheekim@gist.ac.kr

$\nu \approx 1$  for  $\alpha_{\text{LR}} = 9/4$ . Previous quantum Monte Carlo (QMC) calculations with stochastic series expansion [58] provided lower values of  $\nu$  and  $\beta$  in its examined range of  $\alpha_{\text{LR}} \geq 2$ . However, these TDVP and DMRG results all together suggest an interesting possibility that some of the exponents can still be very close to the SR Ising values even for a small  $\alpha_{\text{LR}}$  where the central charge indicates a deviation.

The same scenario was proposed in the study of the Kitaev chain with LR pairing [61, 62] which becomes equivalent to the Ising chain only in the SR limit. Along the critical line of a positive chemical potential, the conformal invariance is broken for  $\alpha_{\text{LR}} < 2$  while the Ising exponent  $\beta$  is unchanged in the test of a quantity that corresponds to the Ising order parameter in the SR limit. Although there is no rigorous mapping between the Kitaev chain and the Ising model at a finite  $\alpha_{\text{LR}}$ , the empirical similarity between the scenario of conformal symmetry breakdown in the Kitaev chain and the previous observations in AF-LR-TFIM motivates us to revisit the phase transition in this LR Ising system to examine the breakdown of the Ising universality and the conformal invariance in different numerical approaches.

Our VMC+RBM calculations investigate this scenario. In the finite-size scaling (FSS) analysis of the order parameter extracted from the ground-state RBM wave function for  $0.5 \leq \alpha_{\text{LR}} \leq 3$ , we find that our estimates of the critical exponents are indeed very close to the SR Ising values for all the values of  $\alpha_{\text{LR}}$  examined, which is in agreement with the previous DMRG results [55, 56]. On the other hand, we find that the exponent of the correlation function and the estimate of the central charge exhibit deviations from the SR Ising values for a small  $\alpha_{\text{LR}}$ . Although an increasing numerical difference in the central charge is observed for a small  $\alpha_{\text{LR}}$  between our estimate extracted from the second Rényi entropy under periodic boundary conditions (PBC) and the previous measurement with the von Neumann entropy in an open chain [53, 54], both results agree on the deviation found at  $\alpha < 1$ , supporting the scenario of conformal invariance breakdown occurring at a sufficiently small  $\alpha_{\text{LR}}$ .

To identify the threshold for the breakdown of the SR Ising class beyond the implications of the critical exponents and the central charge, we additionally examine the critical Binder ratio [40] and the CFT description of the universal form of the correlation function [64]. Both tests show a clear signal of such breakdown at  $\alpha_{\text{LR}} < 2$ , which strengthens the similar evidence found in the measurement of the critical exponent of the correlation function. However, above  $\alpha_{\text{LR}} = 2$ , the detailed view of the scaled correlation function [64] still indicates a gradual deviation from the asymptotic line predicted by the CFT, raising a possibility that a precise value of the threshold can be above  $\alpha_{\text{LR}} = 2$  while it is less than  $\alpha_{\text{LR}} = 3$  where the description of the CFT is well verified.

This paper is organized as follows. The AF-LR-TFIC model Hamiltonian and the numerical details of the VMC+RBM calculations are described in Sec. II. The main results are given in Sec. III. In the subsections, the FSS analysis for the estimate of the critical exponents and the extraction of the central charge from the second Rényi entropy are presented, and then the test of the critical Binder ratio and the comparison with the CFT

prediction of the correlation function are given to identify the threshold. The conclusions are given in Sec. IV.

## II. MODEL AND VMC+RBM CALCULATIONS

We consider the AF-LR-TFIC Hamiltonian [53] given as

$$\hat{H} = \sin \theta \sum_{i < j} J_{ij} \hat{\sigma}_i^x \hat{\sigma}_j^x + \cos \theta \sum_i \hat{\sigma}_i^z, \quad (1)$$

where  $\theta$  is in the range of  $0 < \theta < \pi/2$  for the AF coupling, and the site indices  $i$  and  $j$  run from 1 to  $L$  in the chain of length  $L$ . We impose PBC as the boundary conditions that are necessary for the test of the CFT description of the correlation function constructed in a cylindrical space-time geometry. In the implementation of the algebraically decaying LR interaction under PBC, we choose to write  $J_{ij}$  with a range cutoff that increases with the system size  $L$  by adopting the formulation used in the LR-Kitaev chain [61, 62] as

$$J_{ij} = \begin{cases} |i - j|^{-\alpha_{\text{LR}}} & \text{for } |i - j| < L/2, \\ (L - |i - j|)^{-\alpha_{\text{LR}}} & \text{for } |i - j| > L/2. \end{cases} \quad (2)$$

We choose RBM as an ansatz of a trial wave function for VMC simulations to find an approximate ground state [5]. A trial state can be written as  $|\Psi\rangle = \sum_{\mathbf{s}} \Psi(\mathbf{s}; \mathcal{W}) |\mathbf{s}\rangle$  with the visible variables  $\mathbf{s} = (s_1, s_2, \dots, s_L)$  of RBM, where  $s_i$  indicates  $\sigma_i^x$  for the  $\hat{\sigma}^x$ -basis representation of the given Hamiltonian. We impose the translation symmetry under PBC to reduce the number of variational parameters. Following the procedures of Ref. [5], after integrating out the hidden layer, one can express the RBM wave function as

$$\Psi(\mathbf{s}; \mathcal{W}) = e^{a \sum_{j=1}^L s_j} \prod_{m=1}^L \prod_{i=1}^{n_h} \cosh \left[ b_i + \sum_{j=1}^L W_{ij} T_m(s_j) \right], \quad (3)$$

where the translation operator  $T$  is defined as  $T_m(s_j) = s_{j+m}$  with periodicity  $s_{j+L} = s_j$ , and  $n_h$  is the number of filters given for the symmetry. On a diagram of RBM, one may illustrate the hidden layer with  $N_h = Ln_h$  neurons with  $L$ -fold degeneracy of the neural variables enforcing the translation invariance. In Eq. (3), there are  $(1 + n_h + Ln_h)$  RBM parameters of  $\mathcal{W} \equiv \{a, \mathbf{b}, \mathbf{W}\}$  to be optimized using the VMC method. We adopt complex-valued parameters as suggested in Ref. [5] for better convergence, although the TFIC Hamiltonian is stoquastic [65]. We initialize the RBM by setting  $a = 0$  and assigning Gaussian random numbers with zero mean and variance of  $1/(Ln_h)$  to  $\mathbf{b}$  and  $\mathbf{W}$ .

In VMC calculations, we optimize the RBM parameters using the stochastic reconfiguration (SR) method to construct the natural gradient [66–68]. The SR method can be described as the imaginary-time evolution of a trial state, providing a new state projected in the space of  $\{|\Psi\rangle, \partial_1|\Psi\rangle, \partial_2|\Psi\rangle, \dots\}$ , where  $\partial_i|\Psi\rangle \equiv \frac{\partial|\Psi\rangle}{\partial \mathcal{W}_i}$ . These procedures propose an update of the variational parameter as  $\mathcal{W}_i^{\text{new}} = \mathcal{W}_i^{\text{old}} + \gamma_{\text{SR}} \delta \mathcal{W}_i$ , where  $\delta \mathcal{W}_i$  is determined by solving the linear equation  $\mathbf{S} \delta \mathcal{W} = -\mathbf{f}$ .

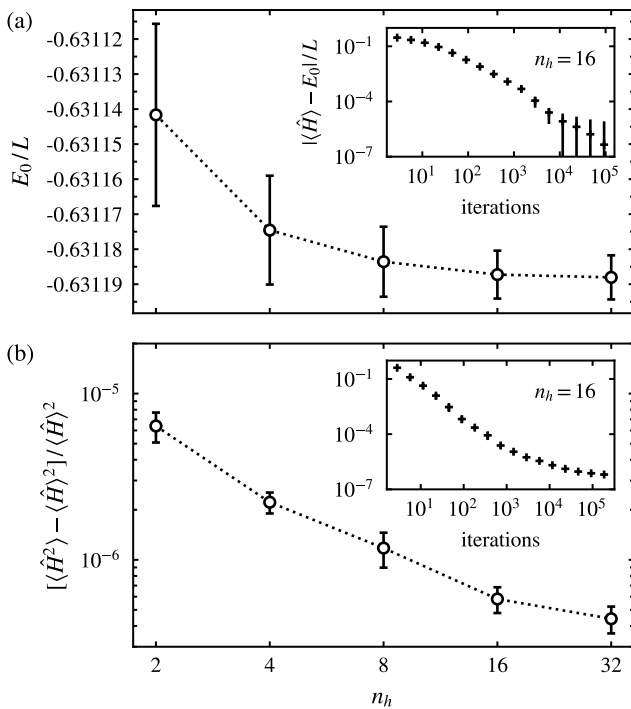


FIG. 1. Convergence test of the the RBM wave function in the VMC search for the ground state. The case with the system of the size  $L = 64$  for  $\alpha_{\text{LR}} = 0.5$  is shown for example. The estimates of (a) energy density  $E_0/L$  and (b) relative variance  $(\langle \hat{H}^2 \rangle - \langle \hat{H} \rangle^2) / \langle \hat{H} \rangle^2$  measured after  $2 \times 10^5$  SR updates are plotted as a function of  $n_h$ . The insets show the same quantities for a fixed number of filters  $n_h = 16$  monitored during the SR iterations of the parameter updates. The data points in the insets represent the averages measured in the logarithmic bins of iteration numbers. The error bars are measured with ten independent RBM wave function samples.

The essential numerical procedures are to evaluate the overlap matrix  $\mathbf{S}$  and the force vector  $\mathbf{f}$ ,

$$S_{ij} = \langle \Delta_i^* \Delta_j \rangle_{\text{mc}} - \langle \Delta_i^* \rangle_{\text{mc}} \langle \Delta_j \rangle_{\text{mc}}, \quad (4)$$

$$f_i = \langle \Delta_i^* E_{\text{loc}} \rangle_{\text{mc}} - \langle \Delta_i^* \rangle_{\text{mc}} \langle E_{\text{loc}} \rangle_{\text{mc}}, \quad (5)$$

where the derivative  $\Delta_i$  and the local energy  $E_{\text{loc}}$  are

$$\Delta_i \equiv \frac{\partial_i \Psi(\mathbf{s}; \mathcal{W})}{\Psi(\mathbf{s}; \mathcal{W})} \quad \text{and} \quad E_{\text{loc}} \equiv \sum_{s'} \langle s | \hat{H} | s' \rangle \frac{\Psi(s'; \mathcal{W})}{\Psi(\mathbf{s}; \mathcal{W})}. \quad (6)$$

The expression  $\langle A \rangle_{\text{mc}} \equiv \sum_{\mathbf{s}} P(\mathbf{s}) A(\mathbf{s})$  denotes the Monte Carlo (MC) measurement of  $A(\mathbf{s})$  with probability  $P(\mathbf{s}) \propto |\Psi(\mathbf{s}; \mathcal{W})|^2$ . We use the conjugate gradient algorithm with the Jacobi preconditioner to solve the linear equation without explicitly storing the  $S$  matrix following the strategy to reduce computational costs proposed in Ref. [68]. For numerical stability, we use the regularization scheme introduced in Ref. [5], where at the  $p$ -th SR iteration,  $S_{ij}$  is replaced by  $S_{ij}(1 + \lambda_p \delta_{ij})$  with  $\lambda_p = \max(\lambda_0 b^p, \lambda_{\text{min}})$ . We use the parameters  $\lambda_0 = 100$ ,  $b = 0.9$ , and  $\lambda_{\text{min}} = 0.01$ . The learning rate  $\gamma_{\text{SR}}$  is initially set to 0.1 and increased by 0.1 for every 10000 SR iterations until it becomes unity.

We monitor the convergence of  $|\Psi\rangle$  to the ground state by evaluating  $\langle \hat{H} \rangle$  and the relative variance defined as

$$\tilde{\sigma}_E \equiv \frac{\langle \hat{H}^2 \rangle - \langle \hat{H} \rangle^2}{\langle \hat{H} \rangle^2}. \quad (7)$$

The relative variance  $\tilde{\sigma}_E$  should be precisely zero when  $|\Psi\rangle$  becomes an exact eigenstate. However, in practice, it does not decrease below a certain value in VMC simulations. Probable systematic causes may include the limited expressive power of a finite-size neural network with a finite  $n_h$ , despite the universal approximation theorem, and the stochastic fluctuations in MC measurements that can affect the linear solver.

Figure 1 presents an example of the convergence test performed at the critical point in the system of size  $L = 64$  for the LR exponent  $\alpha_{\text{LR}} = 0.5$ . Convergence tends to slow down as  $\alpha_{\text{LR}}$  decreases in this LR-AF system. At the critical point, it typically takes about an order of  $10^5$  SR iterations until the energy and variance become saturated within the scale of their fluctuations over the iterations. We find that the accuracy level indicated by  $\tilde{\sigma}_E$  after saturation depends essentially on the number of filters  $n_h$ . In our VMC calculations for the ground state, we set the convergence criterion as  $\tilde{\sigma}_E < 10^{-6}$ , which, for example, is achieved for  $n_h > 8$  in Fig. 1. In our tests,  $n_h = 16$  suffices for system sizes up to  $L = 128$  and for the values of  $\alpha_{\text{LR}}$  that we consider in this study.

### III. RESULTS AND DISCUSSIONS

Using the RBM wave function  $\Psi(\mathbf{s})$  obtained in the VMC optimizations at a given  $\theta$ , we measure the moments of staggered magnetization including the AF order parameter, the two-point correlation function, and the second Rényi entanglement entropy. For a given RBM sample, the MC averages are calculated with  $4 \times 10^8$  configurations of  $\mathbf{s}$  sampled from the probability distribution  $P(\mathbf{s}) \propto |\Psi(\mathbf{s})|^2$  using the Metropolis algorithm. We obtain ten RBM wave function samples from independent VMC calculations. We find that the standard error of the measurement based on one RBM sample is typically smaller than the sample-to-sample fluctuations, and thus we estimate the error bar by the standard deviation of the measurements over the RBM samples.

In this section, we first present the FSS analysis to estimate the critical exponents and the central charge for comparison with the previous TDVP and DMRG results. Then, we proceed to present our additional tests with the critical Binder ratio and the universal form of the correlation function to identify the threshold for the breakdown of the SR Ising universality and the conformal symmetry.

#### A. Order parameter and critical exponents

The emergence of the AF order can be detected by measuring the staggered magnetization in the input layer of the RBM. In the AF phase, the operator  $\hat{M}_s = \sum_i (-1)^i \hat{\sigma}_i^x$  in each parity sector of the  $\mathbb{Z}_2$  symmetry indicates a finite positive or

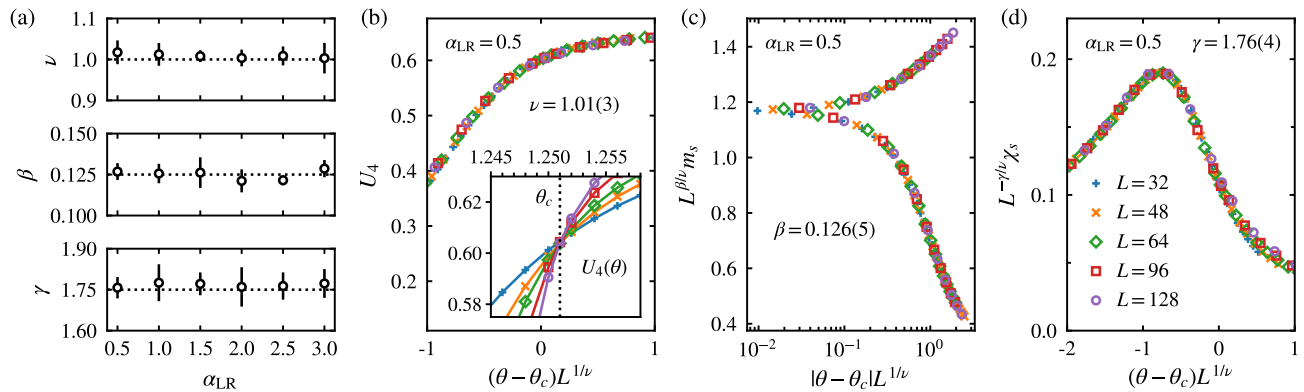


FIG. 2. FSS analysis of RBM observables. (a) The estimates of the critical exponents  $\nu$ ,  $\beta$ ,  $\gamma$  are plotted in the range of  $\alpha_{\text{LR}}$  between 0.5 and 3. The dotted lines are given for comparison with the SR Ising values. The FSS collapse tests with the critical exponents are demonstrated at  $\alpha_{\text{LR}} = 0.5$  for the data of (b) the Binder's cumulant  $U_4$ , (c) the AF order parameter  $m_s$ , and (d) the susceptibility  $\chi_s$ . The inset of (b) shows the crossing point of  $U_4$  locating the critical point  $\theta_c$ .

negative expectation value. Although our MC sampling does not fix the parity, an alternative quantity  $M_s(\mathbf{s}) = |\sum_i (-1)^i s_i|$  can characterize the order-disorder phase transition at the level of the RBM wave function. We write the order parameter as

$$m_s = \frac{1}{L} \langle M_s \rangle_{\text{mc}}. \quad (8)$$

Near a critical point  $\theta_c$ , the order parameter measured in a finite system of size  $L$  is expected to behave asymptotically as  $m_s(\theta, L) \sim L^{-\beta/\nu} \mathcal{M}_0^{(\pm)}(|\theta - \theta_c|L^{1/\nu})$  with the critical exponents  $\beta$  and  $\nu$ , where  $\mathcal{M}_0^{(\pm)}$  is a size-independent scaling function. The corresponding susceptibility can also be defined by the fluctuations of  $M_s$  as

$$\chi_s = \langle M_s^2 \rangle_{\text{mc}} - \langle M_s \rangle_{\text{mc}}^2, \quad (9)$$

which is expected to follow the FSS ansatz of  $\chi_s(\theta, L) \sim L^{\gamma/\nu} \mathcal{X}_0((\theta - \theta_c)L^{1/\nu})$  associated with the exponent  $\gamma$ .

First we determine the critical point  $\theta_c$  for a given  $\alpha_{\text{LR}}$  by locating a crossing point of the Binder's fourth-order cumulant,

$$U_4 = 1 - \frac{\langle M_s^4 \rangle_{\text{mc}}}{3 \langle M_s^2 \rangle_{\text{mc}}^2}, \quad (10)$$

between the curves of different  $L$ 's. The FSS ansatz of the cumulant is given as  $U_4(\theta, L) \sim \mathcal{U}_0((\theta - \theta_c)L^{1/\nu})$ . Although  $\mathcal{U}_0$  becomes independent of  $L$  for a large  $L$ , a finite-size correction can appear for small  $L$ 's. The finite-size correction of the leading order is usually assumed to be in the form of  $\theta_{L,2L}^* - \theta_c \propto L^{-\tilde{\omega}}$  for a crossing point  $\theta_{L,2L}^*$  identified between two adjacent curves of system sizes  $L$  and  $2L$ . We determine  $\theta_c$  based on this correction-to-scaling ansatz with the extrapolation to infinite size.

After locating the critical point  $\theta_c$ , we estimate the critical exponents  $\nu$ ,  $\beta$ , and  $\gamma$  by performing the standard FSS analysis with the FSS ansatz of  $m_s$ ,  $\chi_s$ , and  $U_4$  in the critical region. Figure 2 presents an example of the FSS analysis for  $\alpha_{\text{LR}} = 0.5$ , showing that the data points of different  $L$ 's fall well

on a common scaling curve with our estimates of the critical exponents. The numerical estimates of the critical exponents and errors are measured using the pyfssa package [69, 70]. We tabulate our estimate of  $\theta_c$  and the critical exponents in Table I. Within the error bars, our estimates of the critical exponents are very close to the SR Ising values for all the values of  $\alpha_{\text{LR}}$  examined as shown in Fig. 2(a), which is consistent with the previous DMRG results [55, 56].

## B. Second Rényi entropy and central charge

The logarithmic system-size scaling of the entanglement entropy at a critical point in 1D is a useful universal property to measure the central charge of the CFT that characterizes the phase transition [71–73]. In the previous estimate of the central charge using the TDVP [53], DMRG [54], and generalized Hatree-Fock [59] methods, the von Neumann entanglement entropy was examined under open boundary conditions (OBC). Instead, we consider the second Rényi entropy for the measurement using the RBM wave function under PBC. For the bipartition of a system into subsystems  $A$  and  $B$ , the Rényi

$\alpha_{\text{LR}}$	$\theta_c$	$\nu$	$\beta$	$\gamma$	$\eta$	$c_\infty$
3.0	0.8714(7)	1.00(4)	0.128(5)	1.77(5)	0.2510(4)	0.496(5)
2.5	0.9041(6)	1.01(2)	0.122(3)	1.76(5)	0.2491(2)	0.500(4)
2.0	0.9489(7)	1.00(2)	0.121(7)	1.76(7)	0.2518(7)	0.502(5)
1.5	1.012(1)	1.00(1)	0.126(9)	1.77(4)	0.2450(24)	0.508(4)
1.0	1.103(1)	1.01(3)	0.126(6)	1.78(7)	0.2398(35)	0.491(5)
0.5	1.251(1)	1.01(3)	0.127(5)	1.76(4)	0.2363(15)	0.454(8)

TABLE I. List of the critical points and exponents. Critical exponents  $\nu$ ,  $\beta$ , and  $\gamma$  are determined in the FSS analysis of the collapse of the scaling curve. The exponent  $\eta$  is measured from the scaling of the spin-spin correlation function along a fixed  $r/L = 1/4$  at the critical point  $\theta_c$ . The central charge  $c_\infty$  is extracted from the logarithmic scaling of the second Rényi entropy.

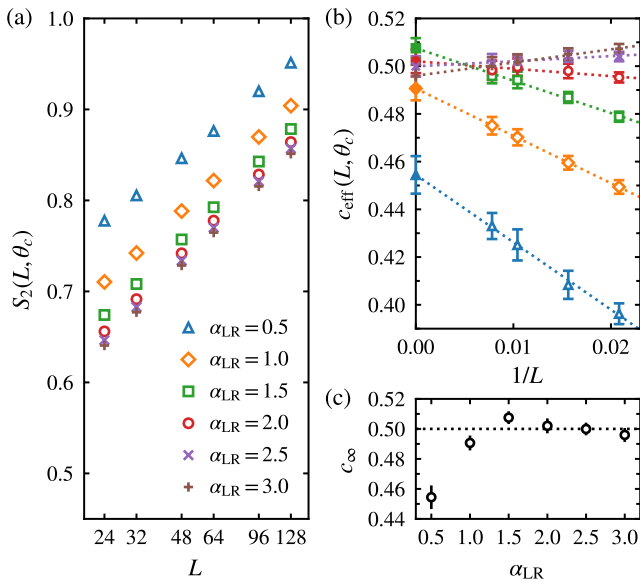


FIG. 3. Estimate of the central charge. (a) The second Rényi entropy  $S_2$  of a half chain is plotted at the critical point  $\theta_c$  as a function of system size  $L$ . (b) The effective central charge  $c_{\text{eff}}(L)$  is extrapolated to determine (c)  $c_\infty$  for the estimate of the central charge.

entanglement entropy of an order  $n$  for  $\rho_A$  is written as

$$S_n(\rho_A) = \frac{1}{1-n} \ln \text{tr} \rho_A^n, \quad (11)$$

where  $\rho_A \equiv \text{tr}_B \rho$  is the reduced density matrix of  $A$  for a pure state  $\rho$ . The von Neumann entropy is recovered at the limit of  $n = 1$ . For the universality class fixed by the CFT, the von Neumann and Rényi entropies at the critical point indicate the same central charge  $c$  in the leading-order FSS behavior. For PBC, the asymptotic scaling behavior of  $S_n$  [73] for half-chain bipartition is written as

$$S_n = \frac{c}{6} \left( 1 + \frac{1}{n} \right) \ln L + c'_n, \quad (12)$$

where  $c'_n$  is a nonuniversal constant.

The second Rényi entropy  $S_2$  can be reliably measured in QMC calculations by using the replica trick [74], which has been successfully applied to the VMC calculations with the RBM wave function [13]. We consider only  $S_2$ , but a method was proposed to compute  $S_n$  of the higher  $n$  and to approximate  $S_1$  in a different NQS representation [75]. Measuring  $S_2$  requires two copies of the RBM state, namely  $\mathbf{s}^{(1)}$  and  $\mathbf{s}^{(2)}$ , sampled from the joint probability distribution  $P(\mathbf{s}^{(1)}, \mathbf{s}^{(2)}) \propto |\Psi(\mathbf{s}^{(1)})|^2 |\Psi(\mathbf{s}^{(2)})|^2$ . Each copy can be rewritten in a bipartite basis of  $\mathbf{s} \equiv (\mathbf{s}_A, \mathbf{s}_B)$ , where  $\mathbf{s}_A$  and  $\mathbf{s}_B$  are associated with the subsystems  $A$  and  $B$ . Then, one can obtain  $e^{-S_2}$  by measuring the swapping operator on  $A$  as

$$e^{-S_2} = \left\langle \frac{\Psi(\mathbf{s}_A^{(2)}, \mathbf{s}_B^{(1)}) \Psi(\mathbf{s}_A^{(1)}, \mathbf{s}_B^{(2)})}{\Psi(\mathbf{s}_A^{(1)}, \mathbf{s}_B^{(1)}) \Psi(\mathbf{s}_A^{(2)}, \mathbf{s}_B^{(2)})} \right\rangle_{\text{mc}}. \quad (13)$$

We extract the central charge from the asymptotic behavior of  $S_2(L) = \frac{c}{4} \ln L + c'_2$ . To deal with finite-size corrections,

we measure  $S_2$  for two system sizes  $L$  and  $L/2$  to define the effective central charge,

$$c_{\text{eff}}(L) = \frac{4}{\ln 2} [S_2(L) - S_2(L/2)], \quad (14)$$

which would explicitly reveal finite-size behavior. The central charge is then formally written as  $c = c_\infty \equiv \lim_{L \rightarrow \infty} c_{\text{eff}}(L)$ , which can be evaluated by extrapolating  $c_{\text{eff}}(L)$  to infinite  $L$ . Figure 3 describes such extrapolation procedures to evaluate  $c_\infty$  with finite-size data of  $S_2(L)$ . We observe that  $c_{\text{eff}}(L)$  exhibits the power-law convergence of  $|c_{\text{eff}}(L) - c_\infty| \propto 1/L$ . This behavior of  $c_{\text{eff}}(L)$  is consistent with the previous discussion on the finite-size correction of  $L^{-1/\nu}$  in the FSS analysis of the entanglement entropy [76].

Our estimate of  $c_\infty$  shows good agreement with  $c = 1/2$  of the SR Ising class for  $\alpha_{LR} \gtrsim 2$ . For  $\alpha_{LR} = 1.5$  and 1, the values of  $c_\infty$  are still close to  $1/2$  within the deviation of 0.01, but the finite-size corrections become systematic and stronger. For  $\alpha_{LR} = 0.5$ , the deviation of  $c_\infty$  from  $1/2$  is much larger than the error bar, implying the breakdown of the conformal symmetry of the SR Ising class. Our results are obtained from the second Rényi entropy under PBC, providing an interesting comparison with the previous results based on the von Neumann entropy under OBC [53, 54, 59]. All studies agree on a significant deviation from  $1/2$  for  $\alpha_{LR} < 1$ . However, we observe the tendency of  $c_\infty$  to decrease below  $1/2$ , which is in contrast to the increase of  $c$  above  $1/2$  previously observed from the von Neumann entropy under OBC. Although we cannot rule out finite-size influences, the inconsistent trend of  $c$  found in the different measures of entanglement with different boundary conditions may also be related to the breakdown of the conformal symmetry.

### C. Critical Binder ratio

Our RBM estimates of the critical exponents and the central charge are consistent with the combined results of the previous TDVP and DMRG studies, supporting the scenario that the conformal symmetry is broken at a sufficiently small  $\alpha_{LR}$  while some of the critical exponents are very close to the SR Ising values. However, there is still a great uncertainty in finding the threshold value of  $\alpha_{LR}$  for the breakdown of the conformal invariance and the universality class of the SR Ising model. Despite the fact that the deviation in the central charge is visibly large only at  $\alpha_{LR} = 0.5$ , the strong finite-size correction observed at a larger  $\alpha_{LR}$  implies that the threshold can be much larger than  $\alpha_{LR} = 0.5$ . Therefore, we need more reliable indicators that can go beyond the estimates of the critical exponents and central charge to test the breakdown of the SR Ising class and the associated conformal invariance.

For such an alternative indicator, we consider the Binder ratio,  $Q \equiv \langle M_s^2 \rangle_{\text{mc}}^2 / \langle M_s^4 \rangle_{\text{mc}}$ , of the second and fourth moments of the staggered magnetization. The Binder ratio at a critical point exhibits a particular value contributing to the universality of the critical behavior, while the value depends on the boundary conditions and the aspect ratio of the system (see, for instance, Refs. [77, 78] and references therein). The

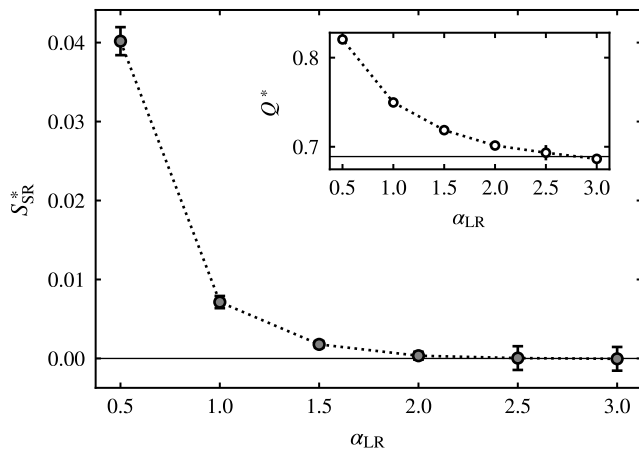


FIG. 4. Test of the critical Binder ratio. The self-combined ratio  $S_{\text{SR}}^*$  and the Binder ratio  $Q^*$  at the critical point are plotted as a function of  $\alpha_{\text{LR}}$ . The data points are extrapolated to infinite size. The horizontal solid lines indicate the SR limit.

critical Binder ratio has been used as a reliable ingredient to identify the universality class in the classical long-range Ising model [40], which inspires us to perform the same test of how the Binder ratio depends on  $\alpha_{\text{LR}}$  for the critical RBM wave function of the AF-LR-TFIC.

In the SR limit, at the exact critical point  $\theta_c = \pi/4$ , we obtain the value of  $Q_{\text{SR}}^* = 0.689(4)$  from the power-law extrapolation of  $Q(L)$  to infinite  $L$ . This particular value of the ratio has not previously been known for the AF-TFIC, but it turns out that the corresponding value of the cumulant  $U_4^* = 0.516(3)$  is very similar to the previous MC estimate of  $U_4^* = 0.514(1)$  reported in the classical 2D Ising model subject to the mixed boundary conditions where the system is periodic in one direction and open in the other direction [79]. The implicit connection between the mixed boundary conditions and the cylindrical geometry of our periodic chain under the imaginary-time evolution at zero temperature may expect the universal value of the Binder ratio in the SR limit.

For a finite  $\alpha_{\text{LR}}$ , we consider the indicator called the self-combined Binder ratio proposed in Ref. [40],

$$S_{\text{SR}}(L) = \frac{1}{Q_{\text{SR}}^*} Q(L) + \frac{1}{Q(L)} Q_{\text{SR}}^* - 2, \quad (15)$$

which removes the leading-order finite-size correction in  $Q(L)$  and thus exhibits better convergence with increasing  $L$  if an accurate value of  $Q_{\text{SR}}^*$  is provided. Figure 4 displays the value of  $S_{\text{SR}}^* \equiv \lim_{L \rightarrow \infty} S_{\text{LR}}(L)$  obtained from the power-law extrapolation to infinite  $L$ . It turns out that while  $S_{\text{SR}}^*$  is almost zero for  $\alpha_{\text{LR}} = 3$  and 2.5, the deviation of  $S_{\text{SR}}^*$  appears for  $\alpha_{\text{LR}} \lesssim 2$  and increases as  $\alpha_{\text{LR}}$  decreases. The estimate of  $Q^* \equiv \lim_{L \rightarrow \infty} Q(L)$  shows a similar increase from the value of the SR limit as  $\alpha_{\text{LR}}$  decreases, although it still indicates a slight deviation even for  $\alpha_{\text{LR}} = 2.5$  and 3 where  $S_{\text{SR}}^* \approx 0$ . This is consistent with the observation in Ref. [40], verifying that  $S_{\text{LR}}(L)$  converges better at a finite  $L$ . Our data suggest that the threshold for the SR Ising universality is possibly around  $\alpha_{\text{LR}} = 2$  above which  $S_{\text{SR}}^*$  is zero within the error bars.

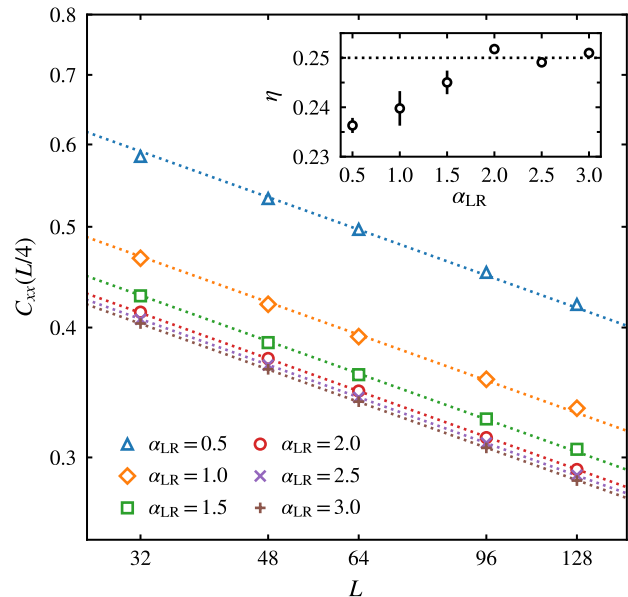


FIG. 5. Critical exponent of the spin-spin correlation function. The correlation function  $C_{xx}(r)$  at  $r = L/4$  is plotted as a function of the system size  $L$ . The inset shows the exponent  $\eta$  extracted from the data fitting to  $C_{xx}(L/4) \propto L^{-\eta}$ . The dotted lines indicating the SR Ising exponent  $\eta = 1/4$  are given for comparison.

#### D. CFT prediction of the correlation function

The other test for the conformal invariance of the SR Ising class concerns the correlation function to compare its asymptotic scaling behavior with the CFT description given at the SR limit, following the strategy proposed in Ref. [64]. The PBC imposed on our RBM wave function is essential for this test. We consider the spin-spin correlation function,

$$C_{xx}(r) = \frac{1}{L-r} \sum_{i=1}^{L-r} \langle \hat{\sigma}_i^x \hat{\sigma}_{i+r}^x \rangle = \frac{1}{L-r} \sum_{i=1}^{L-r} \langle s_i s_{i+r} \rangle_{\text{mc}}, \quad (16)$$

where the distance  $r$  runs from 1 to  $L/2$  in the periodic chain, and the average over the sites is taken for better statistics in the MC measurements.

The CFT in a cylindrical space-time geometry predicts the asymptotic form of the two-point correlation function [80, 81]. In the SR limit, the 2D Ising universality class and its CFT predicts that the correlation function in Eq. (16) behaves as

$$C_{xx}(r) \propto \left( \frac{1}{L \sin(\pi r/L)} \right)^{2\Delta_\sigma} \quad (17)$$

with the scaling dimension  $\Delta_\sigma = 1/8$ . A partial test of this prediction includes verification of the scaling dimension that is equivalent to the exponent  $\eta = 2\Delta_\sigma$  characterizing the algebraic decay of  $C_{xx}(r) \sim r^{-\eta}$  at the critical point. A more comprehensive test is to directly compare the form of the measured correlation function with the description of the CFT. This strategy was originally proposed in the projector QMC

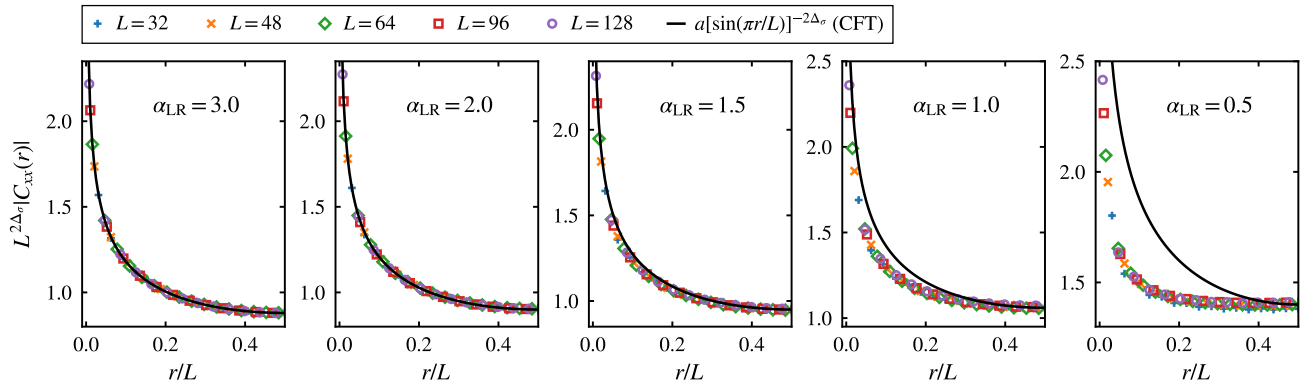


FIG. 6. FSS analysis of the spin-spin correlation function. The data collapse of  $L^{2\Delta_\sigma} |C_{xx}(r)|$  is examined as a function of  $r/L$  with the exponent  $2\Delta_\sigma$  being fixed at the SR Ising value  $1/4$ . The solid line indicates the CFT-predicted form of  $a[\sin(\pi r/L)]^{-2\Delta_\sigma}$  given for comparison with the scaled curve of the measured correlation function.

simulations [64], which we employ here for the RBM wave function obtained in the VMC simulations.

First, we measure the critical exponent  $\eta$  from the FSS behavior of  $C_{xx}(r)$  along a fixed  $r/L = 1/4$ . We obtain the estimate of  $\eta$  from the linear fit to the ansatz of  $C_{xx}(L/4) \propto L^{-\eta}$ , which is displayed as a function of  $L$  on the logarithmic scale in Fig. 5. For  $\alpha_{LR} \geq 2$ , the estimate of  $\eta$  is consistent with the SR Ising value  $1/4$ . However, as  $\alpha_{LR}$  decreases below 2, it turns out that the estimate of  $\eta$  decreases below  $1/4$ , implying that the SR Ising class does not hold below  $\alpha_{LR} = 2$ . These observations are consistent with the previous TDVP result [53], where the threshold value of  $\alpha_{LR} = 2.25$  was suggested based on their estimate of the scaling dimension.

However, it is certainly preferable to find stronger supporting evidence because the numerical deviation of our estimate of  $\eta$  from  $1/4$  is rather small and we cannot rule out finite-size influences in the data fitting. In fact, as shown in Fig. 5, the data points match well with the lines of  $L^{-1/4}$  within the available system sizes. Additionally, assuming that the hyperscaling relation still holds,  $\eta < 1/4$  implies  $\gamma > 7/4$  and  $\beta < 1/8$  if  $\nu = 1$  is fixed. We cannot argue such small changes of the exponents in our FSS analysis of data collapse. Within our limited numerical accuracy, it is thus difficult to precisely determine the breakdown of the universality class solely on the basis of the critical exponents.

For the direct test of the CFT-predicted form of the correlation function in Eq. (17), we perform the FSS analysis with data collapse of  $L^{2\Delta_\sigma} |C_{xx}(r)|$  as shown in Fig. 6. We fix the exponent  $2\Delta_\sigma$  at the SR Ising value  $1/4$  for the test of the SR Ising class. Despite the fact that the measured values of  $\eta$  are not used, we still observe a good collapse of the data points falling on a common scaling curve at all  $\alpha_{LR}$  except with slight deviations found at  $\alpha_{LR} = 0.5$  where  $\eta \approx 0.236$  is maximally different from  $1/4$ . In the graphical comparison between the collapsed data curve and the CFT prediction of  $L^{2\Delta_\sigma} |C_{xx}(r)| \propto [\sin(\pi r/L)]^{-2\Delta_\sigma}$ , we observe that the data curve starts to deviate from the CFT prediction at  $\alpha_{LR} \lesssim 2$ , and the deviations increase with decreasing  $\alpha_{LR}$ , which is consistent with the evidence found in the critical Binder ratio.

To compare the measured correlation function with the CFT

description in higher resolution, we examine the scaled correlation function  $C_{sc}(r/L)$  [64] defined as the ratio of the measured  $C_{xx}(r/L)$  and the form predicted in Eq. (18),

$$C_{sc}(r/L) = \left[ L \sin\left(\pi \frac{r}{L}\right) \right]^{2\Delta_\sigma} |C_{xx}(r)|, \quad (18)$$

where we also fix  $2\Delta_\sigma$  at  $1/4$ . If the CFT of the 2D Ising universality class holds for this LR system, one can expect an asymptotically flat tail in this scaled correlation function. Figure 7 displays  $C_{sc}(r/L)$  for  $\alpha_{LR}$  between 2 and 3. At

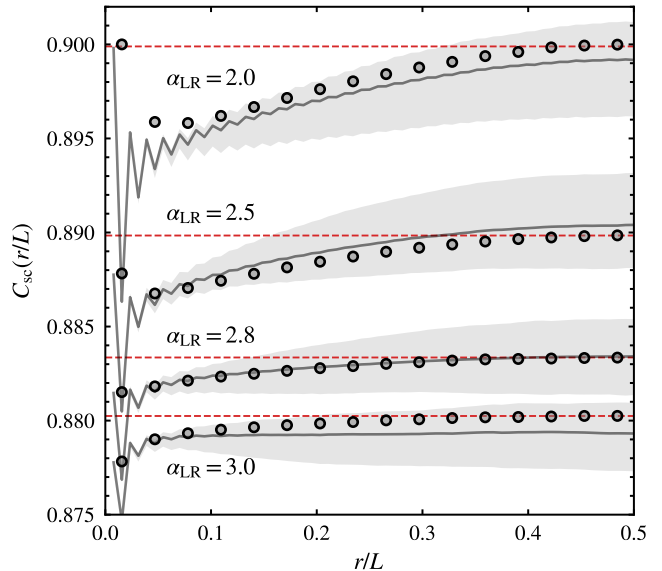


FIG. 7. Scaled correlation function for the test of the CFT description. Equation (18) is examined with ten samples of the RBM wave functions independently obtained in the VMC simulations at the critical point. The markers indicate the data of  $L = 64$  where the fluctuations in the RBM samples are smaller than the marker size. The gray solid line is the average over the samples for  $L = 128$ . The shade is filled between the minimum and maximum magnitudes of the data in the RBM wave function samples for  $L = 128$ .

$\alpha_{LR} = 3$ , one can clearly notice the flat line, which indicates the validity of the CFT description. Although we have not shown here, our test in the SR limit has shown the same flatness of  $C_{sc}(r/L)$  as displayed for  $\alpha_{LR} = 3$  within the fluctuations in the examined RBM samples.

It turns out that the shape of  $C_{sc}(r/L)$  becomes more curved as  $\alpha_{LR}$  decreases. As shown in Fig. 7, the flat tail area in  $C_{sc}(r/L)$  tends to be harder to identify for a smaller  $\alpha$ , such a change in the shape of the correlation function develops gradually as  $\alpha_{LR}$  decreases below 3. Within the achievable accuracy of our present calculations, it is difficult to detect a precise threshold value of  $\alpha_{LR}$  at which the asymptotic flat line would disappear, because fluctuations in RBM samples tend to increase with increasing system size. Our test of  $C_{sc}(r/L)$  suggests that the threshold for the CFT of the SR Ising class may be higher than  $\alpha_{LR} = 2$ , although it still requires much more accurate calculations of the correlation function or more sensitive indicators to identify a precise threshold.

#### IV. SUMMARY AND CONCLUSIONS

We have studied a quantum phase transition in the AF-LR-TFIC using VMC methods with the RBM trial wave function ansatz. Based on the FSS analysis to measure the critical exponents of the order parameter and the estimate of the central charge from the second Rényi entropy, we have verified the previous TVDP and DMRG results [53–56], supporting the scenario [62] that conformal symmetry is broken at a sufficiently small LR exponent  $\alpha_{LR}$  while some critical exponents are very close to the SR Ising values regardless of  $\alpha_{LR}$ . To identify the threshold for the breakdown of the SR Ising universality and the conformal symmetry, we have performed two additional tests that do not rely on the critical exponents and the central charge. Our first test using the self-combined version of the Binder ratio [40] finds that the universal Binder ratio holds for  $\alpha_{LR} \gtrsim 2$  below which the ratio increases significantly as  $\alpha_{LR}$  decreases. In the test for the CFT description of the spin-spin correlation function, our FSS analysis finds a qualitative dif-

ference between the measured data curve and the description of the CFT for  $\alpha_{LR} < 2$ . The detailed view given by the scaled correlation function [64] indicates a gradual change that still occurs above  $\alpha_{LR} = 2$ , raising a possibility that the threshold may be larger than  $\alpha_{LR} = 2$  while it is less than  $\alpha_{LR} = 3$  where the measured data produce the CFT description.

Our measurement of the critical Binder ratio and the test of the CFT-predicted form of the correlation function reveal numerical evidence supporting the breakdown of the Ising universality and the conformal symmetry in the AF-LR-TFIC. However, our rough estimate of the threshold value of  $\alpha_{LR}$  for the breakdown also indicates the need for further intensive studies to precisely determine the threshold with more sensitive indicators of conformal symmetry, such as Klein bottle entropy [82]. In addition, the apparent mismatch between the correlation function exponent and the other critical exponents needs to be further investigated to properly examine the hyperscaling relations with higher numerical accuracy.

Our VMC+RBM calculations for the FSS analysis of the criticality in this LR interacting system exemplify the practical applicability of the NQS framework to the study of quantum phase transitions. While we have only considered a stoquastic Hamiltonian, the accuracy of the RBM wave function shown in our analysis of the critical ground state demonstrates its potential as an alternative or complementary tool to conventional zero-temperature methods.

#### ACKNOWLEDGMENTS

J.K. and D.K. contributed equally to this work. We thank Syngye Todo and Hong-Hao Tu for fruitful discussions in the ASG meeting at the PCS-IBS. This work was supported by the Basic Science Research Program through the National Research Foundation of Korea (NRF-2019R1F1A106321) and also by the KIAS associate member program. Computing resources are provided by the KISTI supercomputing center (KSC-2021-CRE-0165). We appreciate APCTP and PCS-IBS for their hospitality during the completion of this work.

- 
- [1] G. Carleo, I. Cirac, K. Cranmer, L. Daudet, M. Schuld, N. Tishby, L. Vogt-Maranto, and L. Zdeborová, Machine learning and the physical sciences, *Rev. Mod. Phys.* **91**, 045002 (2019).
  - [2] J. Carrasquilla, Machine learning for quantum matter, *Adv. Phys.* **5**, 1797528 (2020).
  - [3] J. Carrasquilla and G. Torlai, How to use neural networks to investigate quantum many-body physics, *PRX Quantum* **2**, 040201 (2021).
  - [4] A. Dawid, J. Arnold, B. Reuena, A. Gresch, M. Płodzień, K. Donatella, K. A. Nicoli, P. Stornati, R. Koch, M. Büttner, R. Okuła, G. Muñoz-Gil, R. A. Vargas-Hernández, A. Cervera-Lierta, J. Carrasquilla, V. Dunjko, M. Gabrié, P. Huembeli, E. van Nieuwenburg, F. Vicentini, L. Wang, S. J. Wetzel, G. Carleo, E. Greplová, R. Krems, F. Marquardt, M. Tomza, M. Lewenstein, and A. Dauphin, Modern applications of machine learning in quantum sciences, arXiv:2204.04198.
  - [5] G. Carleo and M. Troyer, Solving the quantum many-body problem with artificial neural networks, *Science* **355**, 602 (2017).
  - [6] Y. Nomura, A. S. Darmawan, Y. Yamaji, and M. Imada, Restricted Boltzmann machine learning for solving strongly correlated quantum systems, *Phys. Rev. B* **96**, 205152 (2017).
  - [7] H. Saito, Solving the bose–hubbard model with machine learning, *J. Phys. Soc. Jpn.* **86**, 093001 (2017).
  - [8] M. Schmitt and M. Heyl, Quantum many-body dynamics in two dimensions with artificial neural networks, *Phys. Rev. Lett.* **125**, 100503 (2020).
  - [9] A. Nagy and V. Savona, Variational quantum monte carlo method with a neural-network ansatz for open quantum systems, *Phys. Rev. Lett.* **122**, 250501 (2019).
  - [10] M. J. Hartmann and G. Carleo, Neural-network approach to dissipative quantum many-body dynamics, *Phys. Rev. Lett.* **122**, 250502 (2019).
  - [11] F. Vicentini, A. Biella, N. Regnault, and C. Ciuti, Variational



- neural-network ansatz for steady states in open quantum systems, *Phys. Rev. Lett.* **122**, 250503 (2019).
- [12] N. Yoshioka and R. Hamazaki, Constructing neural stationary states for open quantum many-body systems, *Phys. Rev. B* **99**, 214306 (2019).
- [13] G. Torlai, G. Mazzola, J. Carrasquilla, M. Troyer, R. Melko, and G. Carleo, Neural-network quantum state tomography, *Nature Phys.* **14**, 447 (2018).
- [14] G. Torlai, B. Timar, E. P. L. van Nieuwenburg, H. Levine, A. Omran, A. Keesling, H. Bernien, M. Greiner, V. Vuletić, M. D. Lukin, R. G. Melko, and M. Endres, Integrating neural networks with a quantum simulator for state reconstruction, *Phys. Rev. Lett.* **123**, 230504 (2019).
- [15] Y. Nomura and M. Imada, Dirac-type nodal spin liquid revealed by refined quantum many-body solver using neural-network wave function, correlation ratio, and level spectroscopy, *Phys. Rev. X* **11**, 031034 (2021).
- [16] A. Chen, K. Choo, N. Astrakhantsev, and T. Neupert, Neural network evolution strategy for solving quantum sign structures, *Phys. Rev. Res.* **4**, L022026 (2022).
- [17] A. Szabó and C. Castelnovo, Neural network wave functions and the sign problem, *Phys. Rev. Res.* **2**, 033075 (2020).
- [18] T. Westerhout, N. Astrakhantsev, K. S. Tikhonov, M. I. Katsnelson, and A. A. Bagrov, Generalization properties of neural network approximations to frustrated magnet ground states, *Nat. Commun.* **11**, 1593 (2020).
- [19] F. Ferrari, F. Becca, and J. Carrasquilla, Neural gutzwiller-projected variational wave functions, *Phys. Rev. B* **100**, 125131 (2019).
- [20] K. Choo, T. Neupert, and G. Carleo, Two-dimensional frustrated  $J_1$ - $J_2$  model studied with neural network quantum states, *Phys. Rev. B* **100**, 125124 (2019).
- [21] X. Liang, W.-Y. Liu, P.-Z. Lin, G.-C. Guo, Y.-S. Zhang, and L. He, Solving frustrated quantum many-particle models with convolutional neural networks, *Phys. Rev. B* **98**, 104426 (2018).
- [22] K. Choo, A. Mezzacapo, and G. Carleo, Fermionic neural-network states for ab-initio electronic structure, *Nat. Commun.* **11**, 2368 (2020).
- [23] D. Pfau, J. S. Spencer, A. G. D. G. Matthews, and W. M. C. Foulkes, Ab initio solution of the many-electron schrödinger equation with deep neural networks, *Phys. Rev. Res.* **2**, 033429 (2020).
- [24] J. Hermann, Z. Schätzle, and F. Noé, Deep-neural-network solution of the electronic Schrödinger equation, *Nat. Chem.* **12**, 891 (2020).
- [25] D.-L. Deng, X. Li, and S. Das Sarma, Quantum entanglement in neural network states, *Phys. Rev. X* **7**, 021021 (2017).
- [26] J. Chen, S. Cheng, H. Xie, L. Wang, and T. Xiang, Equivalence of restricted Boltzmann machines and tensor network states, *Phys. Rev. B* **97**, 085104 (2018).
- [27] I. Glasser, N. Pancotti, M. August, I. D. Rodriguez, and J. I. Cirac, Neural-network quantum states, string-bond states, and chiral topological states, *Phys. Rev. X* **8**, 011006 (2018).
- [28] Y. Levine, O. Sharir, N. Cohen, and A. Shashua, Quantum entanglement in deep learning architectures, *Phys. Rev. Lett.* **122**, 065301 (2019).
- [29] O. Sharir, A. Shashua, and G. Carleo, Neural tensor contractions and the expressive power of deep neural quantum states, *Phys. Rev. B* **106**, 205136 (2022).
- [30] N. Defenu, T. Donner, T. Macrì, G. Pagano, S. Ruffo, and A. Trombettoni, Long-range interacting quantum systems, *arXiv:2109.01063*.
- [31] C. Monroe, W. C. Campbell, L.-M. Duan, Z.-X. Gong, A. V. Gorshkov, P. W. Hess, R. Islam, K. Kim, N. M. Linke, G. Pagano, P. Richerme, C. Senko, and N. Y. Yao, Programmable quantum simulations of spin systems with trapped ions, *Rev. Mod. Phys.* **93**, 025001 (2021).
- [32] R. Islam, E. E. Edwards, K. Kim, S. Korenblit, C. Noh, H. Carmichael, G.-D. Lin, L.-M. Duan, C.-C. Joseph Wang, J. K. Freericks, and C. Monroe, Onset of a quantum phase transition with a trapped ion quantum simulator, *Nat. Commun.* **2**, 377 (2011).
- [33] J. Zhang, G. Pagano, P. W. Hess, A. Kyprianidis, P. Becker, H. Kaplan, A. V. Gorshkov, Z.-X. Gong, and C. Monroe, Observation of a many-body dynamical phase transition with a 53-qubit quantum simulator, *Nature* **551**, 601 (2017).
- [34] B.-W. Li, Y.-K. Wu, Q.-X. Mei, R. Yao, W.-Q. Lian, M.-L. Cai, Y. Wang, B.-X. Qi, L. Yao, L. He, Z.-C. Zhou, and L.-M. Duan, Probing critical behavior of long-range transverse-field Ising model through quantum Kibble-Zurek mechanism, *PRX Quantum* **4**, 010302 (2023).
- [35] S. Sachdev, *Quantum Phase Transitions*, 2nd ed. (Cambridge University Press, New York, 2011).
- [36] N. Defenu, A. Codello, S. Ruffo, and A. Trombettoni, Criticality of spin systems with weak long-range interactions, *J. Phys. A: Math. Theor.* **53**, 143001 (2020).
- [37] J. Sak, Recursion relations and fixed points for ferromagnets with long-range interactions, *Phys. Rev. B* **8**, 281 (1973).
- [38] E. Luijten and H. W. J. Blöte, Boundary between long-range and short-range critical behavior in systems with algebraic interactions, *Phys. Rev. Lett.* **89**, 025703 (2002).
- [39] M. C. Angelini, G. Parisi, and F. Ricci-Tersenghi, Relations between short-range and long-range ising models, *Phys. Rev. E* **89**, 062120 (2014).
- [40] T. Horita, H. Suwa, and S. Todo, Upper and lower critical decay exponents of ising ferromagnets with long-range interaction, *Phys. Rev. E* **95**, 012143 (2017).
- [41] C. Behan, L. Rastelli, S. Rychkov, and B. Zan, Long-range critical exponents near the short-range crossover, *Phys. Rev. Lett.* **118**, 241601 (2017).
- [42] A. W. Sandvik, Ground states of a frustrated quantum spin chain with long-range interactions, *Phys. Rev. Lett.* **104**, 137204 (2010).
- [43] S. Fey, S. C. Kapfer, and K. P. Schmidt, Quantum criticality of two-dimensional quantum magnets with long-range interactions, *Phys. Rev. Lett.* **122**, 017203 (2019).
- [44] J. Koziol, S. Fey, S. C. Kapfer, and K. P. Schmidt, Quantum criticality of the transverse-field ising model with long-range interactions on triangular-lattice cylinders, *Phys. Rev. B* **100**, 144411 (2019).
- [45] S. Humeniuk, Thermal Kosterlitz–Thouless transitions in the  $1/r^2$  long-range ferromagnetic quantum Ising chain revisited, *J. Stat. Mech.* **2020**, 063105.
- [46] M. F. Paulos, S. Rychkov, B. C. van Rees, and B. Zan, Conformal invariance in the long-range Ising model, *Nuclear Physics B* **902**, 246 (2016).
- [47] A. Dutta and J. K. Bhattacharjee, Phase transitions in the quantum Ising and rotor models with a long-range interaction, *Phys. Rev. B* **64**, 184106 (2001).
- [48] M. Knap, A. Kantian, T. Giamarchi, I. Bloch, M. D. Lukin, and E. Demler, Probing real-space and time-resolved correlation functions with many-body ramsey interferometry, *Phys. Rev. Lett.* **111**, 147205 (2013).
- [49] N. Defenu, A. Trombettoni, and S. Ruffo, Criticality and phase diagram of quantum long-range  $O(N)$  models, *Phys. Rev. B* **96**, 104432 (2017).
- [50] A. Langheld, J. A. Koziol, P. Adelhardt, S. C. Kapfer, and K. P. Schmidt, Scaling at quantum phase transitions above the upper

- critical dimension, *SciPost Phys.* **13**, 088 (2022).
- [51] Z. Zhu, G. Sun, W.-L. You, and D.-N. Shi, Fidelity and criticality of a quantum Ising chain with long-range interactions, *Phys. Rev. A* **98**, 023607 (2018).
- [52] S. Shiratani and S. Todo, Stochastic approximation analysis of dynamical quantum critical phenomena in long-range transverse-field Ising chain, arXiv:2305.14121.
- [53] T. Koffel, M. Lewenstein, and L. Tagliacozzo, Entanglement entropy for the long-range Ising chain in a transverse field, *Phys. Rev. Lett.* **109**, 267203 (2012).
- [54] D. Vodola, L. Lepori, E. Ercolessi, and G. Pupillo, Long-range Ising and Kitaev models: phases, correlations and edge modes, *New J. Phys.* **18**, 015001 (2016).
- [55] G. Sun, Fidelity susceptibility study of quantum long-range antiferromagnetic Ising chain, *Phys. Rev. A* **96**, 043621 (2017).
- [56] R. Puebla, O. Marty, and M. B. Plenio, Quantum Kibble-Zurek physics in long-range transverse-field Ising models, *Phys. Rev. A* **100**, 032115 (2019).
- [57] S. Fey and K. P. Schmidt, Critical behavior of quantum magnets with long-range interactions in the thermodynamic limit, *Phys. Rev. B* **94**, 075156 (2016).
- [58] J. A. Koziol, A. Langheld, S. C. Kapfer, and K. P. Schmidt, Quantum-critical properties of the long-range transverse-field Ising model from quantum Monte Carlo simulations, *Phys. Rev. B* **103**, 245135 (2021).
- [59] M. P. Kaicher, D. Vodola, and S. B. Jäger, Mean-field treatment of the long-range transverse field Ising model with fermionic gaussian states, *Phys. Rev. B* **107**, 165144 (2023).
- [60] J. C. Halimeh, M. Van Damme, L. Guo, J. Lang, and P. Hauke, Dynamical phase transitions in quantum spin models with antiferromagnetic long-range interactions, *Phys. Rev. B* **104**, 115133 (2021).
- [61] D. Vodola, L. Lepori, E. Ercolessi, A. V. Gorshkov, and G. Pupillo, Kitaev chains with long-range pairing, *Phys. Rev. Lett.* **113**, 156402 (2014).
- [62] L. Lepori, D. Vodola, G. Pupillo, G. Gori, and A. Trombettoni, Effective theory and breakdown of conformal symmetry in a long-range quantum chain, *Ann. Phys.* **374**, 35 (2016).
- [63] T. Kuwahara and K. Saito, Area law of noncritical ground states in 1D long-range interacting systems, *Nat. Commun.* **11**, 4478 (2020).
- [64] P. Patil, Y. Tang, E. Katz, and A. W. Sandvik, Indicators of conformal field theory: Entanglement entropy and multiple-point correlators, *Phys. Rev. B* **96**, 045140 (2017).
- [65] C.-Y. Park and M. J. Kastoryano, Expressive power of complex-valued restricted Boltzmann machines for solving nonstoquastic Hamiltonians, *Phys. Rev. B* **106**, 134437 (2022).
- [66] S. Sorella, Generalized lanczos algorithm for variational quantum monte carlo, *Phys. Rev. B* **64**, 024512 (2001).
- [67] S. Sorella, M. Casula, and D. Rocca, Weak binding between two aromatic rings: Feeling the van der Waals attraction by quantum Monte Carlo methods, *J. Chem. Phys.* **127**, 014105 (2007).
- [68] E. Neuscamman, C. J. Umrigar, and G. K.-L. Chan, Optimizing large parameter sets in variational quantum monte carlo, *Phys. Rev. B* **85**, 045103 (2012).
- [69] A. Sorge, pyfssa 0.7.6. zenodo (2015).
- [70] O. Melchert, autoscale.py - a program for automatic finite-size scaling analyses: A user's guide, arXiv:0910.5403.
- [71] G. Vidal, J. I. Latorre, E. Rico, and A. Kitaev, Entanglement in quantum critical phenomena, *Phys. Rev. Lett.* **90**, 227902 (2003).
- [72] P. Calabrese and J. Cardy, Entanglement entropy and quantum field theory, *J Stat. Mech.* **2004**, P06002.
- [73] P. Calabrese and J. Cardy, Entanglement entropy and conformal field theory, *J. Phys. A: Math. Theor.* **42**, 504005 (2009).
- [74] M. B. Hastings, I. González, A. B. Kallin, and R. G. Melko, Measuring Renyi entanglement entropy in quantum Monte Carlo simulations, *Phys. Rev. Lett.* **104**, 157201 (2010).
- [75] Z. Wang and E. J. Davis, Calculating Rényi entropies with neural autoregressive quantum states, *Phys. Rev. A* **102**, 062413 (2020).
- [76] M. Campostrini, A. Pelissetto, and E. Vicari, Finite-size scaling at quantum transitions, *Phys. Rev. B* **89**, 094516 (2014).
- [77] V. Privman, *Finite Size Scaling and Numerical Simulation of Statistical Systems* (World Scientific, Singapore, 1990).
- [78] W. Selke, The critical Binder cumulant for isotropic Ising models on square and triangular lattices, *J. Stat. Mech.* **2007**, P04008.
- [79] W. Selke, Critical Binder cumulant of two-dimensional Ising models, *Eur. Phys. J. B* **51**, 223–228 (2006).
- [80] M. Henkel, *Conformal Invariance and Critical Phenomena* (Springer-Verlag, Berlin Heidelberg, 1999).
- [81] P. Francesco, P. Mathieu, and D. Sénéchal, *Conformal Field Theory* (Springer Science & Business Media, New York, 2012).
- [82] H.-H. Tu, Universal entropy of conformal critical theories on a Klein bottle, *Phys. Rev. Lett.* **119**, 261603 (2017).